Solid State Communications 377 (2024) 115366

Contents lists available at ScienceDirect

Solid State Communications

journal homepage: www.elsevier.com/locate/ssc

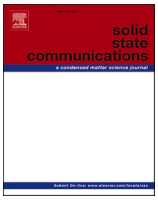

# Structural stability, opto-electronic, magnetic and thermoelectric properties of half-metallic ferromagnets quaternary Heusler alloys CoFeXAs (X = Mn, Cr and V)

K. Bouferrache [a], M.A. Ghebouli [b], Y. Slimani [c], B. Ghebouli [d], M. Fatmi [b,*], T. Chihi [b], Norah Algethami [e], Saif A. Mouhammad [e], Sultan Alomairy [e], Elkenany B. Elkenany [f,g]

[a] Physics Department, Faculty of Sciences, University of Mohamed Boudiaf, M'sila, 28000, Algeria
[b] Research Unit on Emerging Materials (RUEM), University Ferhat Abbas of Setif 1, Setif, 19000, Algeria
[c] Laboratory of Intelligent System (LSI), Faculty of Technology, University Ferhat Abbas of Setif 1, Setif, 19000, Algeria
[d] Laboratory for the Study of Surfaces and Interfaces of Solid Materials (LESIMS), University Ferhat Abbas of Setif 1, Setif, 19000, Algeria
[e] Physics Department, College of Science, Taif University, P.O. Box 11099, Taif, 21944, Saudi Arabia
[f] Physics Department, Faculty of Sciences, Mansoura University, Mansoura, 35516, Egypt
[g] Physics Department, College of science and arts, Najran University, Najran, Saudi Arabia

ARTICLE INFO

Communicated by Ji Chen

*Keywords:*
Heusler alloy
GGA-mBJ
Half metallicity
Ferromagnets
Magnetism

ABSTRACT

The Quaternary Heusler alloys CoFeXAs (X = Cr, Mn and V) fully spin-polarized with half-metallic stability, show low direct band gap, high absorption in the ultraviolet light, high spin polarization and adequate Seebeck coefficient. CoFeCrAs, CoFeMnAs and CoFeVAs have an integer magnetic moment of 4 μB, 5 μB and 3 μB according to the Slater-Pauling rule. The obtained minimal energy favors the type I CoFeVAs alloy over the type III CoFeCrAs and CoFeMnAs alloys. For CoFeCrAs and CoFeMnAs alloys, there is no band gap close to the Fermi level in the minority-spin, suggesting that they are direct Γ–Γ band gap semiconductors. Three-dimensional Co, Fe, and Mn atoms hybridized strongly, with little input from V and As atoms. Co, Fe, Cr, and Mn all have parallel magnetic moments, which results in ferromagnetic interactions between these atoms and gives these elements their ferromagnetic character.

## 1. Introduction

Quaternary Heusler alloys have a particular interest because of their high spin polarization and half-metallic ferromagnets, which enable their use in thermoelectric and spintronic applications [1]. The contribution of valence electrons near the Fermi level in a spin type leads to high spin polarization. Strongly spin-polarized half-metallic ferromagnets materials reveal a metallic behavior for one type of spin and semiconductor character for the other type of spin leading for a good polarization at Fermi level [2]. An example of quaternary Heusler alloys are CoFeXAs (X = Cr, Mn and V), which are synthesized as a combination of the two ternary Heusler alloys $Co_2$(X = Cr, Mn and V) As and $Fe_2$(X = Cr, Mn and V) As. These quaternary Heusler alloys have a prototype of LiMgPdSn structure [3]. Co, Fe and X (X = Cr, Mn and V) elements motivate this computational study of structural, opto-electronic, magnetic and thermoelectric properties of half-metallic ferromagnet (HMF) quaternary Heusler alloys CoFeXAs (X = Cr, Mn and V). The study conducted by X. Dai et al. reports that quaternary Heusler alloy CoFeMnSi is crystallized in the structure with half-metallicity [4]. Goa et al. indicate that CoFeCrAl and CoFeCrSi are ferromagnets with a high semi-metallic band gap [5]. It is cited from research conducted by several researchers on quaternary semi-metallic Heusler, such as Rached et al. [6], Dahmane et al. [7], Wei et al. [8] and Zhang et al. [9]. The high Curie temperature and high magnetic moment of Heusler alloy retain important criteria for technological applications [10,11]. Semi-metallic Heusler magnets are governed by the Slater-Pauling laws, which link the total number of valence electrons to the total spin magnetic moment in the unit cell [12]. The study carried out on CoFeCrAs quaternary Heusler alloy indicates that it is half-metallic ferromagnet in its YI-type structure [13,14]. These semi-metals have advantages for their applications in the magnetic field, since they have a low Gilbert damping parameter and create a high spin-bias current and hence exhibit low energy loss.

* Corresponding author.
*E-mail address:* fatmimessaoud@yahoo.fr (M. Fatmi).

https://doi.org/10.1016/j.ssc.2023.115366
Received 30 May 2023; Received in revised form 17 October 2023; Accepted 18 October 2023
Available online 24 October 2023

**Table 1**
The values of $R_{MT}xK_{max}$, $R_{MT}$ of each constituent and k-meches of CoFeXAs (X = Cr, Mn and V) alloys using GGA.

| type-I | $R_{MT}xKmax$ | $R_{MT}$ (Co) | $R_{MT}$ (Fe) | $R_{MT}$ (X) | $R_{MT}$ (As) | k-meches |
|---|---|---|---|---|---|---|
| CoFeCrAs | 9 | 2.400 | 2.40 | 2.28 | 2.28 | 3000 |
| CoFeMnAs | 9 | 2.34 | 2.34 | 2.34 | 2.29 | 3000 |
| CoFeVAs | 9 | 2.38 | 2.38 | 2.32 | 2.32 | 3000 |

**Table 2**
The effective Coulomb interaction of Co, Fe, Cr and V for CoFeCrAs, CoFeMnAs and CoFeVAs.

| | Co | Fe | Mn | Cr | V |
|---|---|---|---|---|---|
| CoFeCrAs $U_{eff}$ (eV) | 3.49 | 4.66 | 3.80 | 3.35 | 5.09 |
| CoFeMnAs $U_{eff}$ (eV) | 3.56 | 3.08 | | | |
| CoFeVAs $U_{eff}$ (eV) | 1.85 | 3.96 | | | |

Quaternary Heusler alloys CoFeXAs (X = Cr, Mn and V) exhibit adequate thermoelectric properties, such as a flat d band behavior around the Fermi level and large Seebeck coefficient, which make them desirable performances for thermoelectric applications. These alloys under study with half-metallic stability, show good direct band gap in the minority-spin, high conductivity and absorption in the ultraviolet region, high spin polarization, adequate Seebeck coefficient are candidates for use in solar panels, spintronic and thermoelectric device applications. CoFeXAs (X = Cr, Mn et V) Half-Heusler alloys show good thermoelectric characteristics and are known for their mechanical, dynamic and thermodynamic stability. This family of alloys simultaneously exhibits a high Curie temperature (900 K≤), a strong spin polarization at the Fermi level (90%≤) and a high magnetic moment (4 μB≤). CoFeMnAs has a polarization of 100%, a magnetic moment around 5 μB and a curie temperature of 926.2 K. This Heusler is considered an excellent thermoelectric material. While CoFeCrAs having a Curie temperature of 759 K and CoFeVAs of magnetic moment 3 μB do

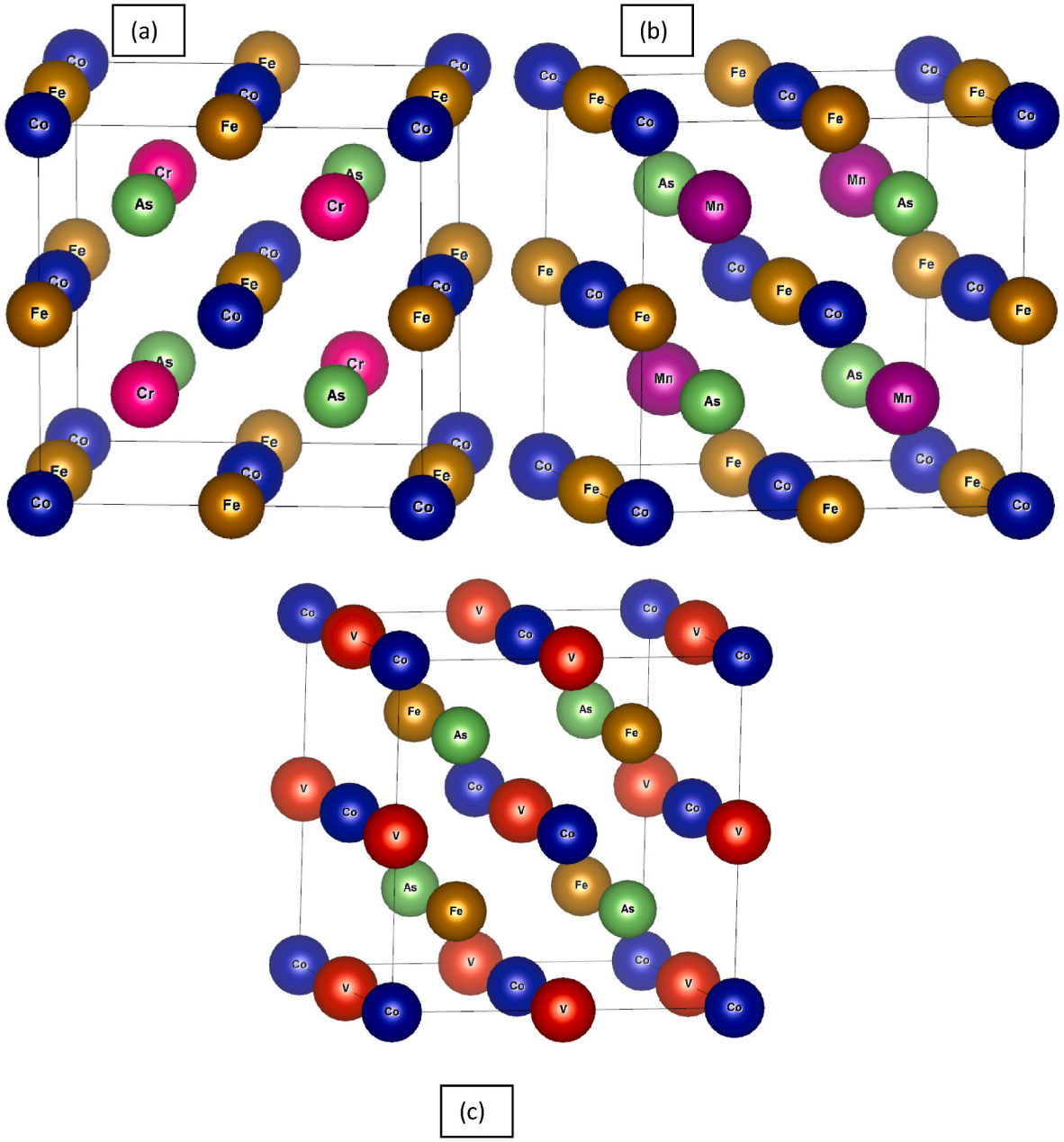


**Fig. 1.** The structural configurations type of CoFeCrAs (a), CoFeMnAs (b) and CoFeVAs (c).

**Table 3**
Atomic occupancy Wyckoff positions XX′YZ for CoFeXAs (X = Cr, Mn and V) quaternary Heusler alloys.

| | | | | |
|---|---|---|---|---|
| type-I | X (0, 0, 0) | X′ (1/4. 1/4, 1/4) | Y (1/2. 1/2, 1/2) | Z (3/4. 3/4, 3/4) |
| type-II | X (1/4. 1/4, 1/4) | X′ (0, 0, 0) | Y (1/2. 1/2, 1/2) | Z (3/4. 3/4, 3/4) |
| type-III | X (0, 0, 0) | X′ (1/2. 1/2, 1/2) | Y (1/4. 1/4, 1/4) | Z (3/4. 3/4, 3/4) |

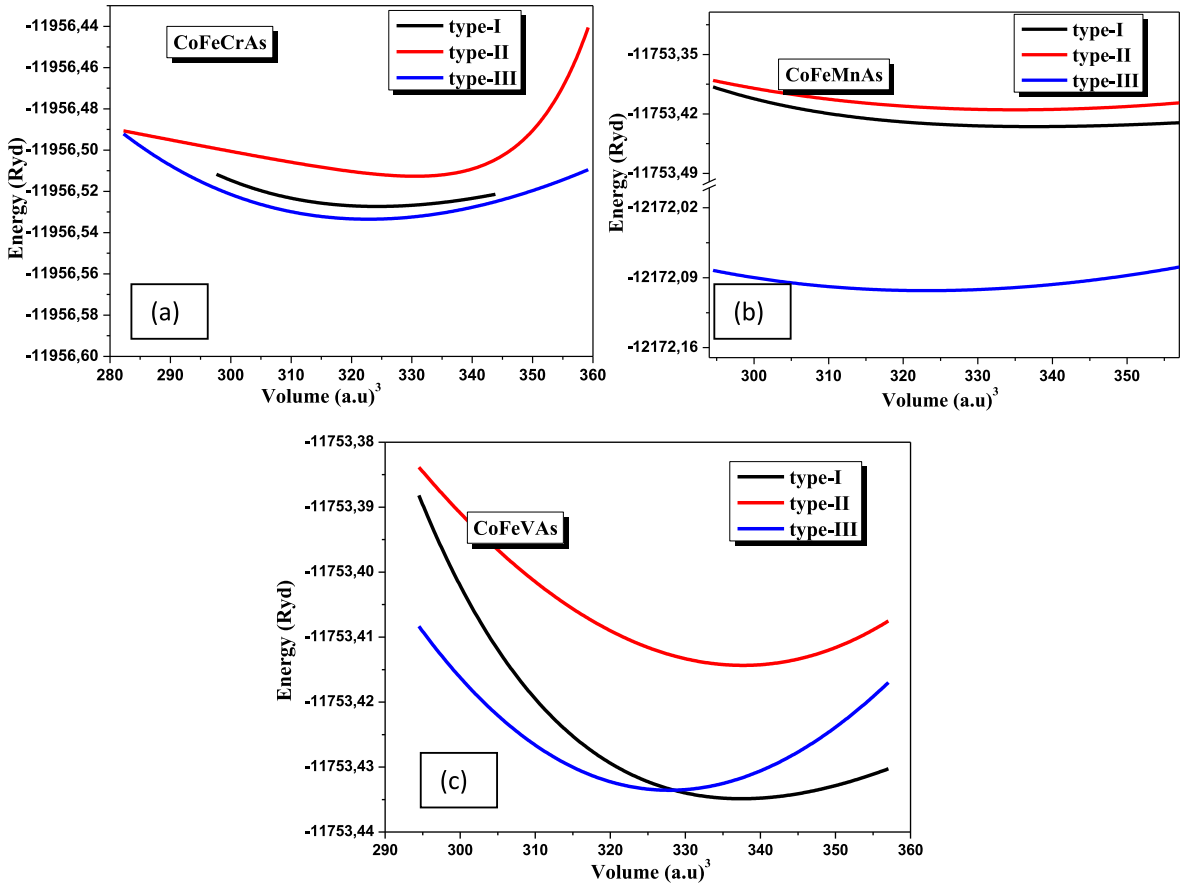


**Fig. 2.** Energy change with respect to volume for (a) CoFeCrAs, (b) CoFeMnAs and (c) CoFeVAs in the ferromagnetic phase.

not satisfy all conditions of thermoelectricity.

## 2. Calculation method

The WIEN2k code's implementation of augmented plane-wave functions plus local orbitals and the GGA-mBJ approximation as exchange potential were used in the calculation process. In the electronic characterisation, the modified Becke-Johnson exchange potential is utilized, and the DFT + U is employed to tackle the electron-electron correlation effect [15–18]. The $R_{MT}xK_{max}$ parameter, the muffin-tin radii ($R_{MT}$) of Co, Fe, Mn, Cr, V and As and k-meshes for the Brillouin zone integration as reported in Table 1 ensure perfect convergence. GGA + U approach. Calculation of the on-site effective Coulomb interaction parameter ($U_{eff}$) of Co, Fe, Mn and Cr between the localized electrons (3d) for CoFeCrAs, CoFeMnAs and CoFeVAs in the augmented plane-wave method are calculated based on the works described in Refs. [19,20]. We adopt a supercell, where one of them is considered an impurity. The addition and removal of an electron from the 3d sub-shell of the impurity atom (Co, Fe, Cr, Mn, V), implies that the number of

**Table 4**
Minimum cohesive energy calculated from equation of state Birch-Murnaghan of Quaternary Heusler CoFeXAs (X = Cr, Mn and V) for Type I, type-II and type-III.

| | type-I | type-II | type-III |
|---|---|---|---|
| CoFeCrAs | −11956.527321 | −11956.510862 | −11956.533498 |
| CoFeMnAs | −12172.076528 | −12172.046400 | −12172.102128 |
| CoFeVAs | −11753.435217 | −11753.414268 | −11753.433579 |

**Table 5**
Lattice constant, bulk modulus and its pressure derivative, minimum cohesive energy and elastic constants of CoFeXAs (X = Cr, Mn and V).

| Alloy | $a_0$ (Å) | B (GPa) | B′ | $E_0$ (Ry) | $C_{11}$ (GPa) | $C_{12}$ (GPa) | $C_{44}$ (GPa) |
|---|---|---|---|---|---|---|---|
| CoFeCrAs | 5.7623 | 199.06 | 3.12 | −11956.533498 | 252.58 | 198.29 | 195.76 |
| | 5.75 [12] | | | | 218.74 [22] | 191.82 [22] | 134.23 [22] |
| CoFeMnAs | 5.7629 | 205.50 | 2.17 | −12172.102128 | 230.46 | 179.39 | 67.15 |
| | 5.74 [12] | | | | 227.26 [23] | 180.82 [23] | 55.28 [23] |
| CoFeVAs | 5.84 | 171.02 | 7.284 | −11753.435217 | 190.10 | 138.34 | 166.15 |
| | 5.78 [12] | | | | | | |

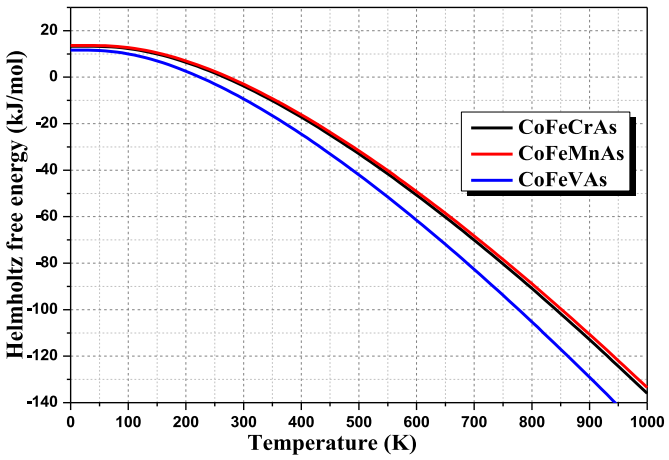


**Fig. 3.** The Helmholtz free energy in the temperature range 0–1000 K for CoFeXAs (X = Cr, Mn and V).

electrons ($n$) in the unhybridized d shell varies and the calculation of $U_{eff}$ is done as follows:

$$U_{eff} = \varepsilon_{3d\uparrow}\left[\frac{n+1}{2}, \frac{n}{2}\right] - \varepsilon_{3d\uparrow}\left[\frac{n+1}{2}, \frac{n}{2} - 1\right] - \varepsilon_F\left[\frac{n+1}{2}, \frac{n}{2}\right] + \varepsilon_F\left[\frac{n+1}{2}, \frac{n}{2} - 1\right] \quad (1)$$

where $\varepsilon_{3d\uparrow}$ and $\varepsilon_F$ represent the spin-up 3d eigenvalue and Fermi energy. The effective parameter $U_{eff} = U - J$ is adopted as an only input parameter, where $U$ and $J$ are the Coulomb and exchange parameters. In this work $J$ has been assumptive set equal 0. The results are reported in Table 2. For the calculation of optical and thermoelectric properties, we use k-meshes = 10,000. The spherical harmonic expansion of maximum $I_{max} = 10$ expresses the charge density and potential. The cut-off energy that separates valence and core states was - 8 Ry and $10^{-3}$ e was used as charge convergence. Although the muffin tin radii ($R_{MT}$) affect the electrical properties, it has a far smaller impact than the mBJ exchange potential. When all of the bonds are broken, the cohesive energy is required to separate the solid into isolated atoms since it translates the solid's binding force. The bulk cohesive energy of the N atoms in the unit cell is given by Ref. [21]:

$$E_{coh}^{GGA-mBJ}(r) = \frac{E_{tot}^{GGA-mBJ}(r) - \sum_N E_{iso}^{GGA-mBJ}}{N} \quad (2)$$

## 3. Results and discussions

### 3.1. Structure and stability

CoFeXAs (X = Cr, Mn and V) quaternary Heusler take the general formula XX′YZ, having a 1:1:1:1 stoichiometry and an *F4-3m* space group. Z is the primary group element and X, X′, and Y are transition metals. They crystallize in III type YI, YII and YIII with the prototype LiMgPdSn-type. The structural configurations of CoFeXAs (X = Cr, Mn and V) were obtained if switching the position of transition metals when As is attached to 4a (0, 0, 0) site as presented in Fig. 1. The atomic occupancy Wyckoff positions XX′YZ for CoFeXAs (X = Cr, Mn and V) quaternary Heusler alloys are reported in Table 3. The physical properties of quaternary Heusler alloys depend on the position of the atoms in the crystal, since a small disorder affects their electronic structure. An order result when atoms occupy their specific sites, therefore the crystal structure is thoroughly studied. An optimization was performed by studying the total spin-polarized energies as a function of volumes as depicted in Fig. 2 for the three type structures of CoFeXAs (X = Cr, Mn and V) in the ferromagnetic phase. We take note that CoFeCrAs and CoFeMnAs are more stable in the type III structure, while the type I is the

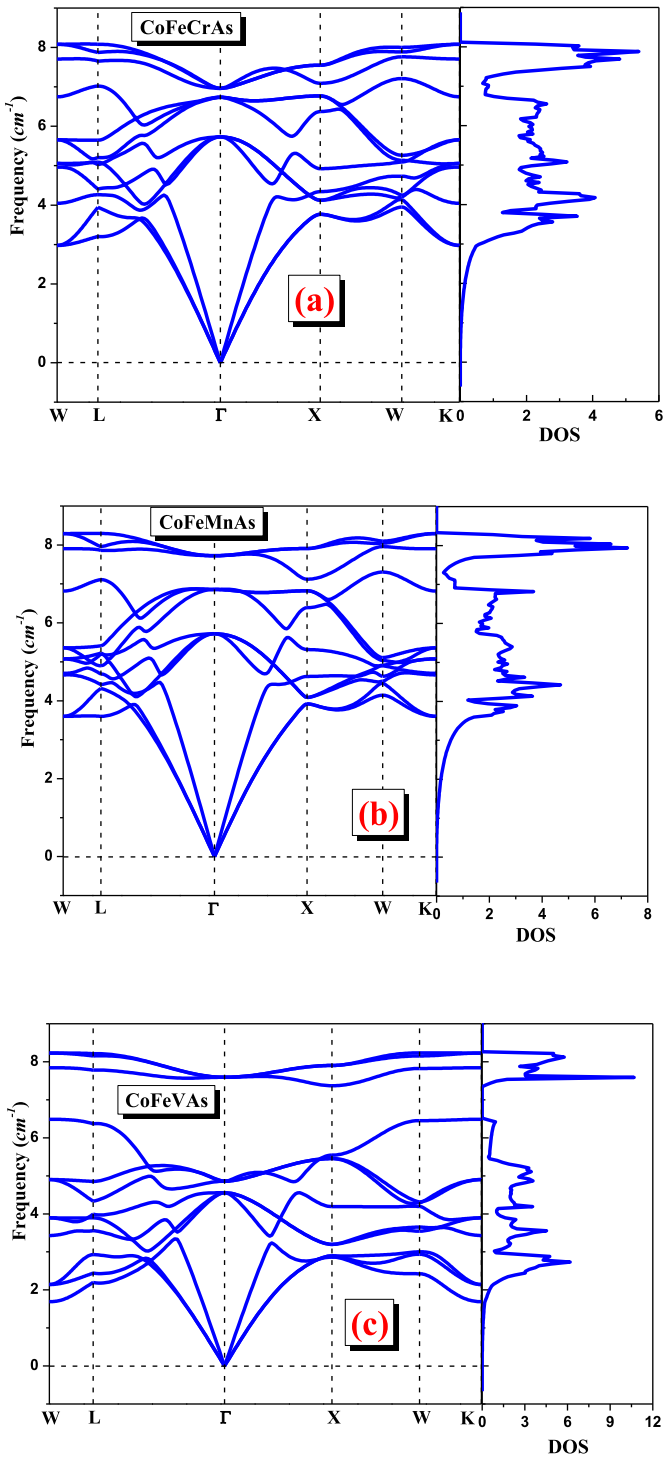


**Fig. 4.** The phonon dispersion curves and total densities of state of CoFeXA (X = Cr, Mn et V).

preferred crystal structure in CoFeVAs. Thus, we treat CoFeCrAs and CoFeMnAs in the type III structure, while CoFeVAs is studied in the type I structure. The minimum cohesive energy calculated from equation of state Birch-Murnaghan as illustrated in Table 4 confirm it. We estimate the optimized lattice constant, the corresponding minimum of cohesive total energy, the bulk modulus and its derivative with respect to the pressure and elastic constants as mentioned in Table 5. No experimental data of structural parameters, cohesive energy and elastic constants are reported in the literature for these three alloys, except the mentioned parameters of CoFeCrAs are compatible with those quoted in the

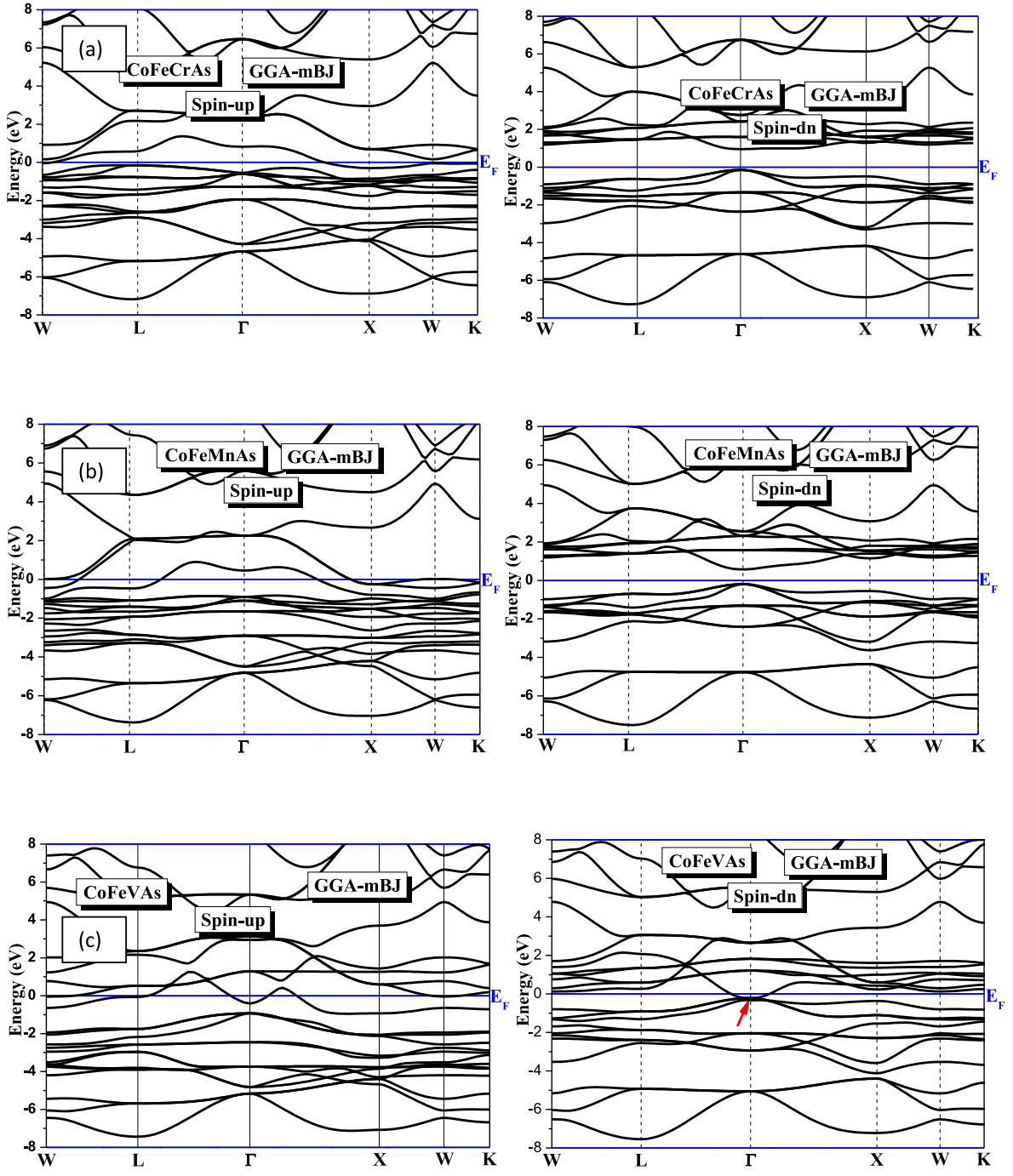


**Fig. 5.** Band structures computed using GGA-mBJ with spin-up and spin-dn for CoFeCrAs (a), CoFeMnAs (b) and CoFeVAs (c).

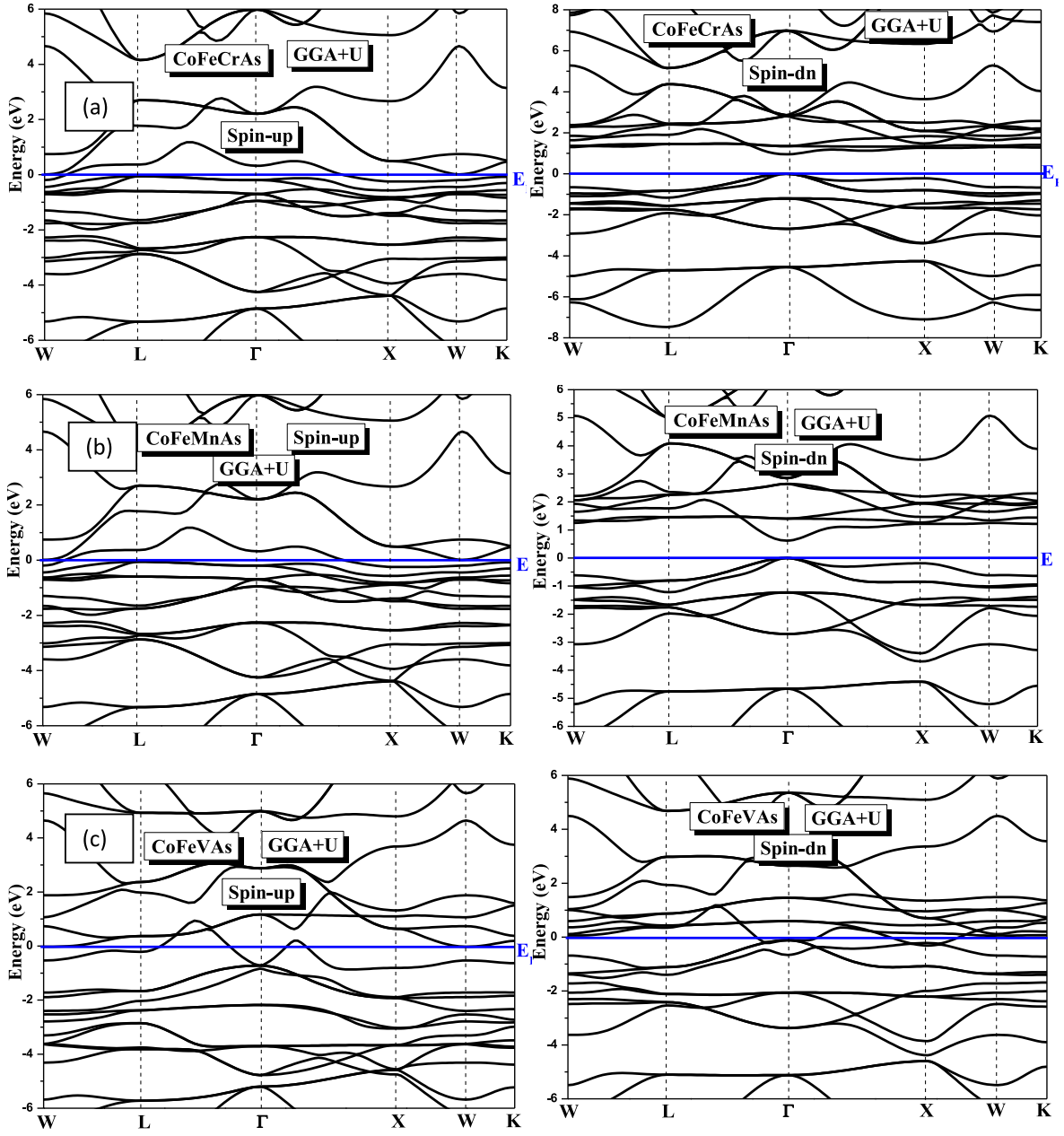


**Fig. 5.** (*continued*).

**Table 6**
The band gap calculated using GGA, EV-GGA, mBJ-GGA and GGA + U for majority-spin and minority-spin in CoFeCrAs, CoFeMnAs and CoFeVAs.

| | GGA | | EV-GGA | | mBJ-GGA | | GGA + U | |
|---|---|---|---|---|---|---|---|---|
| | majority-spin | minority- spin | majority-spin | minority- spin | majority-spin | minority-spin | majority-spin | minority- spin |
| CoFeCrAs | metal | 0.45 eV (Γ–Γ)<br>0.52 [1] | metal | 0.74 eV (Γ–Γ) | metal | 1.10 (Γ–Γ)<br>1.12 [1] | metal | 0.95 (Γ–Γ) |
| CoFeMnAs | metal | 0.12 eV (Γ–Γ) | metal | 0.35 eV (Γ–Γ) | metal | 0.76 eV (Γ–Γ) | metal | 0.62 (Γ–Γ) |
| CoFeVAs | metal | 0<br>0 [27] | metal | 0 | metal | 0 | metal | metal |

literature $a = 5.742$ Å, $a = 5.75$ Å and $a = 5.754$ Å [1,12,13], B = 208 GPa, $B' = 4.47$ and E = −11956.53302 Ry [13]. The theoretical values of elastic constants for CoFeCrAs and CoFeMnAs quoted in the literature agree well with our results [22,23].

The elastic constants satisfy the stability criteria cited below, then these Heuslers are mechanically stable. $C_{11} - C_{12} > 0$ , $C_{11} + 2C_{12} > 0$ , $C_{44} > 0$, $C_{12} < B < C_{11}$ [24]. The chemical potential between atoms substantially influences the formation enthalpy of a solid. As a result, a negative value for the formation enthalpy shows thermodynamic stability in the ground state. The system is more stable the lower the formation enthalpy. CoFeXAs (X = Cr, Mn, and V) Half-Heusler alloys are studied in terms of their elastic constants, enthalpy of formation, and

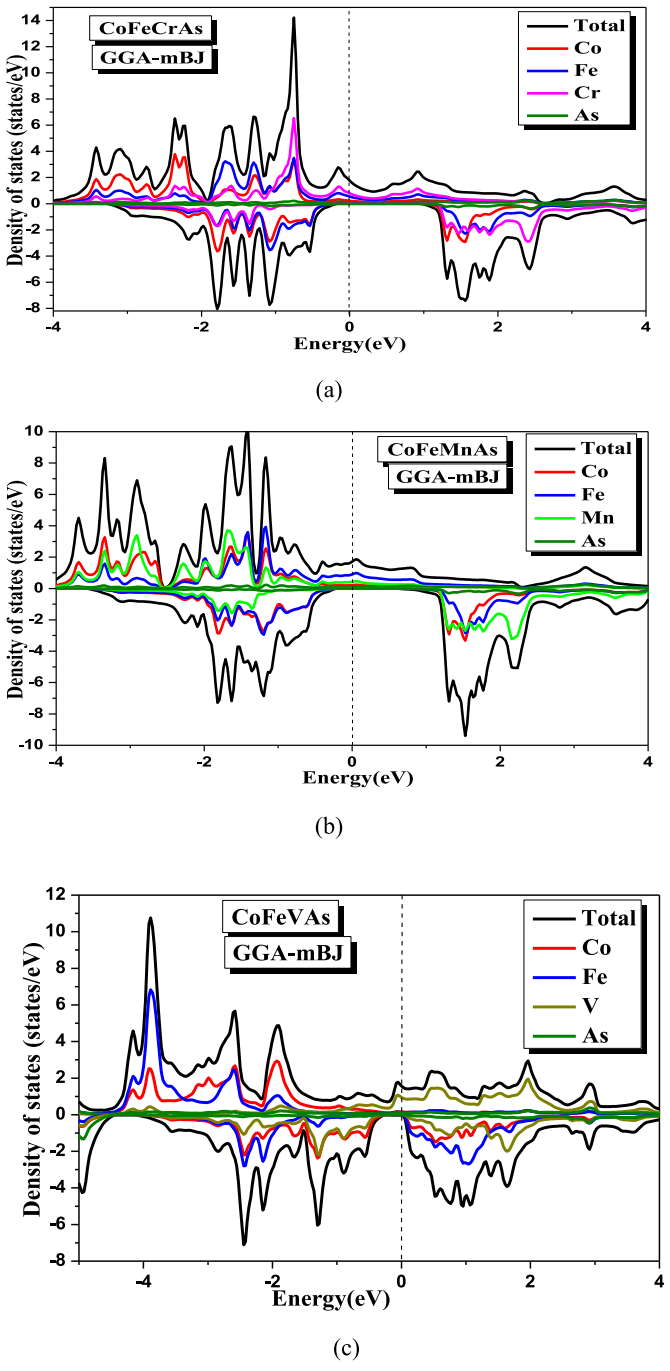


**Fig. 6.** The density of states of (a) CoFeCrAs, (b) CoFeMnAs and (c) CoFeVAs.

phonon dispersion. As shown in Fig. 3, studying the Helmholtz free energy under the impact of temperature in the range of 0–1000 K is necessary to estimate thermodynamic stability. At room temperature, CoFeXAs (X = Cr, Mn, and V) has a negative Helmholtz free energy, which gets less as temperature rises. This finding suggests that these compounds are stable from a thermodynamic perspective. In CoFeVAs, the stability is more obvious. The dynamic stability of CoFeXAs (X = Cr, Mn, and V) is investigated using the phonon dispersion curves and total densities of states, as illustrated in Fig. 4. Due to the absence of fictitious phonon frequencies, these compounds exhibit dynamic stability.

### *3.2. Electronic properties*

The band structure is a determining factor in the estimation of the thermoelectric properties, which are related to the band gap. This energy gap must be estimated with precision, hence the use of the GGA-mBJ potential, which gives a value close to the experimental one [25, 26]. The spin-polarized band structures of CoFeXAs (X = Cr, Mn and V) quaternary Heusler alloys for an equilibrium lattice constant into two spin channels and GGA-mBJ and GGA + U functionals are shown in Fig. 5. Because the energy bands cross the Fermi level at varying locations of symmetry, all of these alloys are half-metallic in the majority-spin (spin-up), including CoFeVAs in the minority-spin (spin-down). For the CoFeCrAs and CoFeMnAs alloys, there is no band around the Fermi level in the minority-spin, suggesting semiconductor characteristics. These two materials are minority-spin direct band gap semiconductors. Table 6 shows the band gap values in both cases of minority and majority spin determined with GGA, GGA-EV, GGA-mBJ and GGA + U, which agree with their theoretical values [1,27]. Understanding the band structure requires the calculation of the total and partial densities of states as a function of energy into two spin channels as illustrated in Figs. 6 and 7. A strong hybridization between 3d-Co, 3d-Fe and 3d-Mn and negligible contribution of V and As atoms are observed. The valence band consists of two areas for the majority-spin and a single area for the minority-spin. The zero value of electronic total density of states (TDOS) in the minority-spin at the Fermi level confirms the semiconducting behavior of CoFeCrAs and CoFeMnAs alloys. For the alloys tested at the Fermi level, the presence of a value of the total electronic density of states in the majority-spin indicates their metallicity. The development of adherent d and anti-adherent d bands with a band gap around the Fermi level results from the hybridization of large valence energy d-states and smaller valence energy d-states. The V and As atoms, on the other hand, have no effect on the band gap. The band structures in the majority-spin overlap slightly on either side of the Fermi level, so CoFeCrAs, CoFeMnAs and CoFeVAs are considered spin gapless semiconductors (SGS). These alloys show a large band gap below the Fermi level in the majority-spin band structures resulting in negligible TDOS. The electronic contribution of Fe, Co and Mn in the case of n-type carriers is dominant for spin-dn.

### 3.3. Optical properties

The light-matter interaction results in three types of photon-energy transformations. In Fig. 8, we show employing the GGA-mBJ functional; the following properties of CoFeCrAs, CoFeMnAs, and CoFeVAs in the majority-spin were calculated: optical conductivity, electron energy loss, real and imaginary portions of the dielectric function, reflectivity, refractive index, and extinction coefficient. All optical properties are determined using the dielectric function's real and imaginary portions. For opto-electronic applications, a material must have direct band gap with plausible interband transitions. The absorption spectra in the studied alloys have the same shape. The maximum of absorption coefficient value is in the range (200–212) x$10^4$ $cm^{-1}$ at about 9 eV, which corresponds to the ultraviolet light. The absorption increases in the sequences CoFeVAs → CoFeMnAs → CoFeCrAs. The studied alloys having a maximum absorption in the ultraviolet region suggest their application as optoelectronic devices operating in this region and as absorber for photovoltaic devices. The effect of photon energy on optical conductivity is investigated under incidence along the crystallographic direction [100] plane. In the conductivity spectrum, there are two flats estimated to be (8000–14,000) $\Omega^{-1}$ $cm^{-1}$ and (4000–8000) $\Omega^{-1}$ $cm^{-1}$, positioned in the ranges (2.5–4.5) eV and (4.5–9) eV. CoFeCrAs and CoFeMnAs have higher optical conductivity. The energy losses brought on by electron contact with the crystal are related to the band structure of the crystal. In the UV, certain alloys experience energy loss. The maximum energy loss is located between (20–25)% at (2.2–2.3) eV, the maximum loss is obtained in CoFeCrAs and CoFeMnAs. The material's nonlinear optical behavior is explained by the real portion of the dielectric function. At roughly 2.8 eV, the actual part's negative value appears. The imaginary part of the dielectric function characterizes the

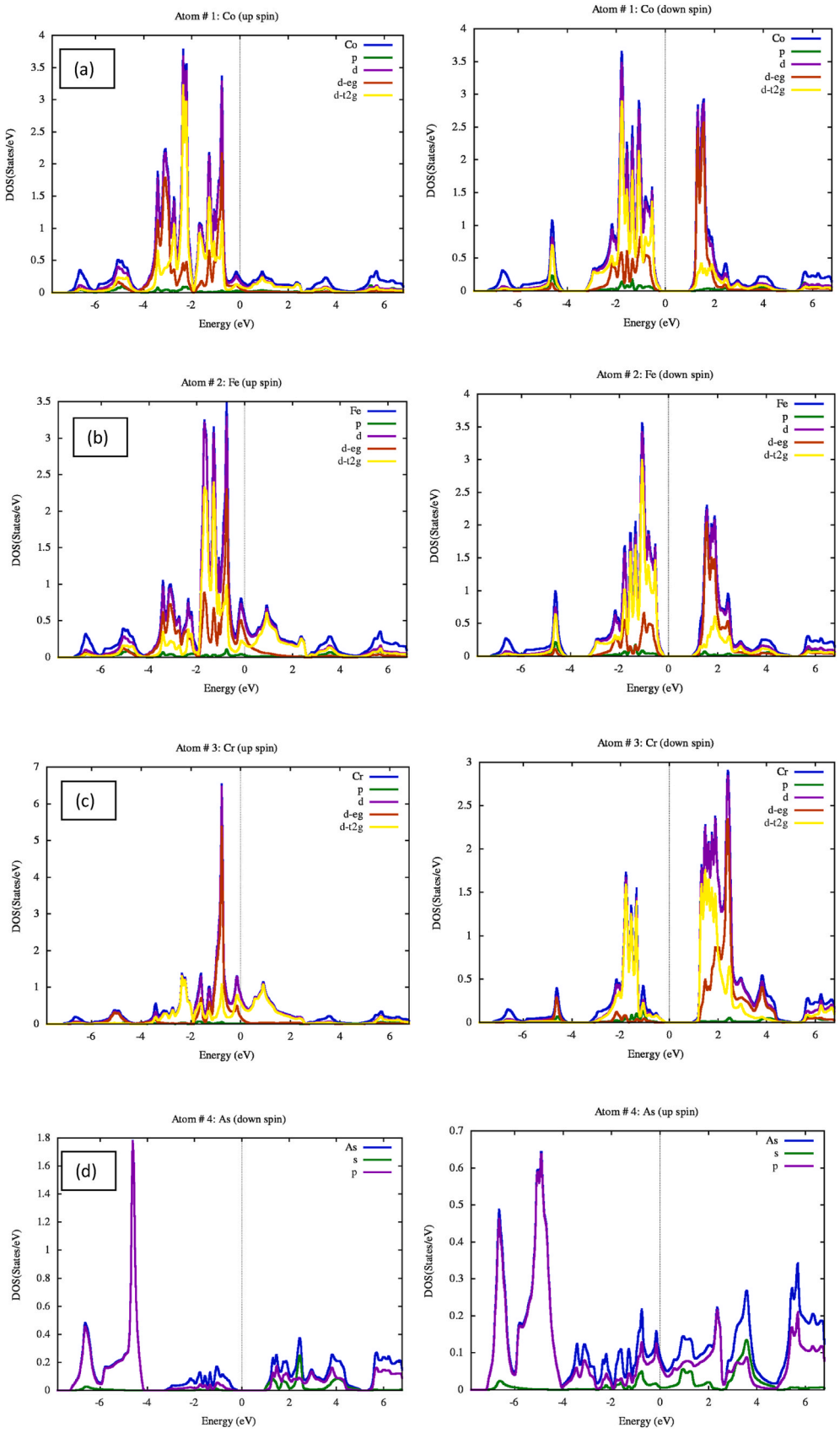


**Fig. 7.** The partial density of states of atoms (a) Co, (b) Fe, (c) Cr and (d) As in CoFeCrAs, CoFeMnAs and CoFeVAs with majority-spin and minority-spin using GGA-mBJ functional.

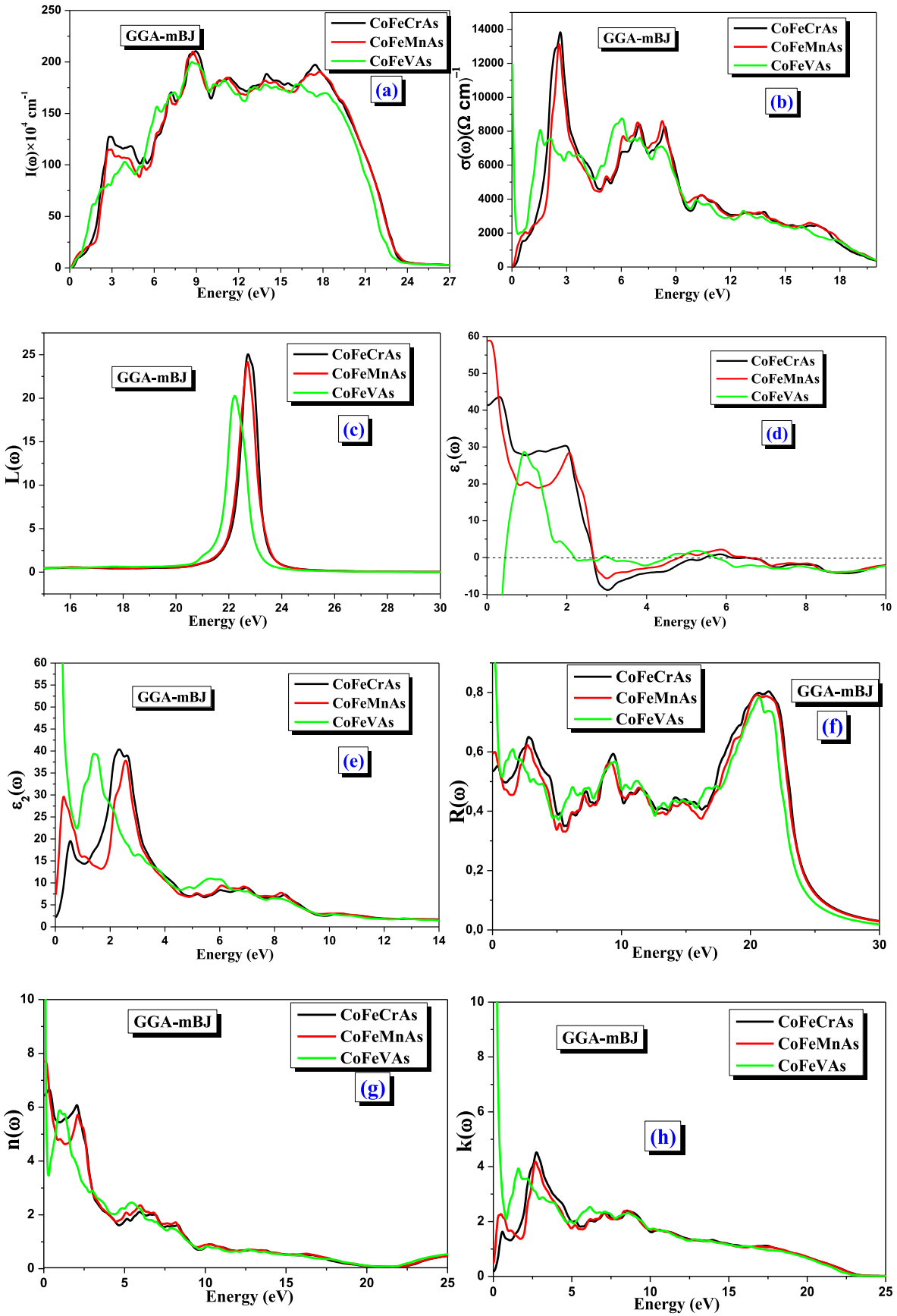


**Fig. 8.** Absorption coefficient (a), optical conductivity (b), energy loss spectra (c), real and imaginary parts of the dielectric function (d) and (e), reflectivity spectra (f), refractive index (g), extinction coefficient (h) as a function of energy for CoFeXAs (X = Cr, Mn and V) using GGA-mBJ.

**Table 7**
Calculated interstitial, molecular, atomic and total magnetic moments for CoFeXAs (X = Cr, Mn and V) alloys.

| | Functional | interstitial | $\mu_{Co}$ ($\mu_B$) | $\mu_{Fe}$ ($\mu_B$) | $\mu_X$ ($\mu_B$) | $\mu_{tot}$ ($\mu_B$) |
|---|---|---|---|---|---|---|
| CoFeCrAs | GGA | 0.05 | 0.99 | 0.85 | 2.089 | 3.99 |
| | | 0.11 [1] | 0.91 [12] | 0.80 [12] | 2.34 [12] | 4.00 [3] |
| | | | 1.02 [1] | 0.69 [1] | 2.16 [1] | 3.9 [1] |
| | EV-GGA | 0.012 | 1.00 | 0.85 | 2.13 | 3.99 |
| | mBJ | −0.062 | 1.12 | 0.88 | 2.05 | 4.00 |
| | GGA + U | 0.16 | 0.82 | 0.82 | 2.16 | 4 |
| **CoFeMnAs** | GGA | −0.008 | 1.007 | 1.07 | 2.93 | 5.03 |
| | | | 0.94 [12] | 0.99 [12] | 3.12 [12] | 5.00 [12] |
| | EV-GGA | −0.08 | 0.96 | 1.01 | 2.98 | 4.85 |
| | mBJ | −0.17 | 1.28 | 0.73 | 3.14 | 5.00 |
| | GGA + U | −0.06 | 1.20 | 0.68 | 3.18 | 5 |
| **CoFeVAs** | GGA | −0.02 | 1.12 | 2.51 | −0.808 0.75 [12] | 2.75 |
| | | | 1.05 [12] | 1.19 [12] | | 3.00 [12] |
| | EV-GGA | −0.08 | 1.28 | 2.68 | −0.954 | 2.88 |
| | mBJ | −0.25 | 1.43 | 2.72 | −0.99 | 2.99 |
| | GGA + U | −0.25 | 1.45 | 2.77 | −0.7 | 3 |

absorption of a material in inter-band transitions from the valence band to the conduction band. A material's capacity to reflect radiation is gauged by its reflectivity. The reflectance reaches multiple peaks and minima in the UV range. Interdiffusion, oxidation, and thermal stability all limit reflectivity. The reflectivity value in CoFeCrAs, CoFeMnAs and CoFeVAs quaternary Heusler alloys is 52%, 60% and 90%. The reflectivity exists at zero frequency because of the lattice vibration inside the crystal. CoFeCrAs reflects 62% in the visible light and 42% in the ultraviolet light. The visible and ultraviolet light donates more than 50% of total energy. These alloys are candidate for photocatalytic water splitting solar-to-hydrogen energy conversion. A material's refractive index gauges its transparency to incoming radiation. When photons flow through a medium with covalently bonded atoms, the refractive index becomes more critical. CoFeCrAs, CoFeMnAs, and CoFeVAs quaternary Heusler alloys have static refractive index values of 6, 7.8, and 9. In a diffusion phenomenon, the extinction coefficient quantifies the strength of the contact. The static extinction coefficient increases in the sequences CoFeCrAs → CoFeMnAs → CoFeVAs. The maximum angle of refraction is observed at 3.5 eV for CoFeCrAs and CoFeMnAs, while, it has a maximum at 2 eV for CoFeVAs. The alloys under study show a low band gap, high conductivity and absorption in the ultraviolet region, which are interesting characteristics in materials for application in solar panels.

### 3.4. Magnetic properties

The link between the quantity of valence electrons and the total spin magnetic moment $Z_{tot}$ with the Slater–Pauling rule is given by $m_{tot} = Z_{tot} - 24$ for full Heusler CoFeXAs (X = Cr, Mn and V). $Z_{tot}$ for CoFeCrAs, CoFeMnAs and CoFeVAs is 28, 29 and 27 [12], so the total magnetic moment is indeed equal to an integer 4 μB, 5 μB and 3 μB and obey to the Slater–Pauling rule for HM ferromagnets [28,29]. Understanding the origin of the spin gapless semiconductors magnetic (SGSM) requires the representation of the energy levels of the band structures (majority-spin) and (minority-spin). The occupied states are localized below the Fermi level and the number in each orbital designates the corresponding degeneracy. When the Slater–Pauling rule follows the relation $m_{tot} = Z_{tot} - 24$, the majority-spin and minority-spin states give a total spin magnetic moment of 3 μB, 4 μB and 5 μB for CoFeVAs, CoFeCrAs and CoFeMnAs. The electrons in the majority-spin band structure inhabit the eu states, and in order to produce a spin-gapless semiconductor, the non-bonding eu bands need not overlap with the antibonding eg states. Table 7 shows the computed interstitial, atomic, and total magnetic moments of CoFeXAs (X = Cr, Mn, and V) alloys using GGA, GGA + EV, mBJ and GGA + U. The $U_{eff}$ effect on magnetic moment was observed in all studied alloys. The total magnetic moment is caused by the partial magnetic moment of each atom as well as the interstitial zone for each alloy. Note that the contribution of vanadium is low for CoFeVAs, while chromium takes the largest part. *As* magnetic moment is close to zero in all alloys, where it's unpolarized. The magnetic moment of vanadium is antiparallel to those of Co and Fe. CoFeCrAs, CoFeMnAs and CoFeVAs have 28, 29 and 27 valence electrons per formula unit. The minority-spin band (N ↓) of CoFeCrAs, CoFeMnAs and CoFeVAs are occupied by twelve (1-s, 3-p and 8-d) electrons, eleven (3-p and 8-d) electrons and nine (3-p and 6-d) electrons. CoFeCrAs and CoFeMnAs present eight electrons from the d states five from bonding (2 × eg and 3 × t2g) and three from non-bonding (3 × t1u). While, CoFeVAs shows six electrons from the d states, three from bonding (2 × eg and 1 × t2g) and three from non-bonding (3 × t1u). The rest of the electrons in CoFeCrAs, CoFeMnAs and CoFeVAs is 16, 18 and 18 occupy the minority-spin band. The magnetic moment of Co, Fe, Cr and Mn are parallel, this induces ferromagnetic interactions between these atoms, and therefore the alloys studied are ferromagnetic in nature. The magnetism in these alloys is explained from their local density of states (LDOS) spectra as shown in Fig. 6. Magnetism in the alloy CoFeCrAs is discussed as an example. The *eg* state splits into two parts because of the anisotropic bond strength between the different pairs of atoms associated with the magnetic ion. In the case of the Fe (Co) atom, the state includes a d-eg subshell located above the Fermi level and d-t2g subshell below the Fermi level in the minority-spin channel. So the Fe (Co) offers 1 μB magnetic moment contribution. For the Cr atom, the *eg* state splits into a d-eg subshell above the Fermi level and a d-t2g subshell below the Fermi level in the majority-spin channel. However, the t2g peak is divided into two parts, the double occupies the part below the Fermi level and the individual

**Table 8**
Total electron density $N(E_F)$ for majority-spin and minority-spin at the Fermi level and spin polarization (SP) for CoFeXAs (X = Cr, Mn and V) alloys.

| Functional | CoFeCrAs | | | CoFeMnAs | | | CoFeVAs | | |
|---|---|---|---|---|---|---|---|---|---|
| | $N(E_F)$ | | SP | $N(E_F)$ | | SP | $N(E_F)$ | | SP |
| | $N(E_F)^{\downarrow}$ | $N(E_F)\uparrow$ | | $N(E_F)^{\downarrow}$ | $N(E_F)\uparrow$ | | $N(E_F)^{\downarrow}$ | $N(E_F)\uparrow$ | |
| GGA | 0.00 | 38.27 | 100% | 0.00 | 24.41 | 100% | 0.11 | 3.67 | 94% |
| EV-GGA | 0.00 | 35.04 | 100% | 0.00 | 25.13 | 100% | 0.03 | 3.68 | 98% |
| GGA-mBJ | 0.00 | 24.30 | 100% | 0.00 | 22.85 | 100% | 0.33 | 20.90 | 96% |

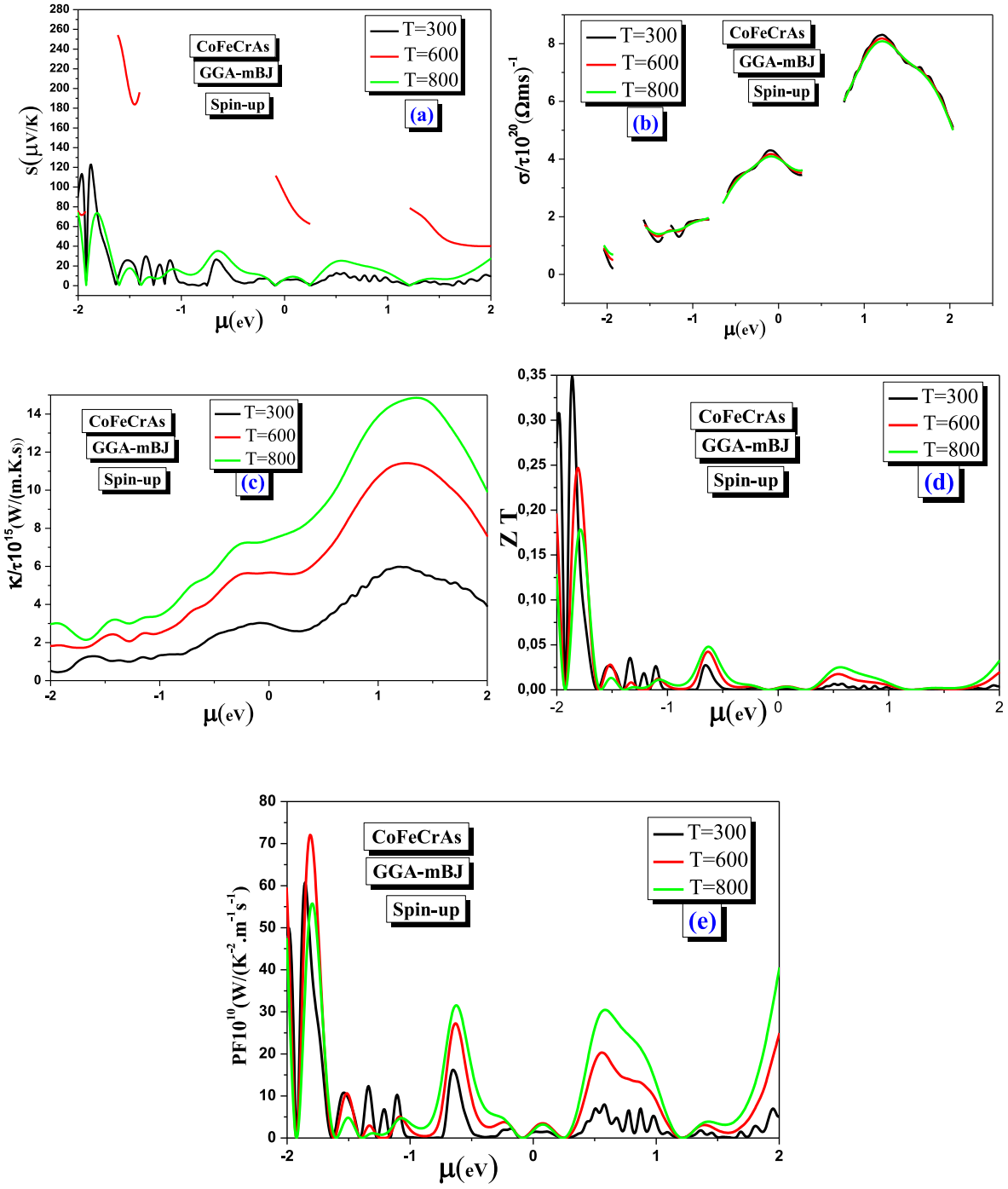


**Fig. 9.** The Seebeck coefficient (a), electrical conductivity (b), electronic thermal conductivity (c), figure of merite (d), Power factor (e) as a function of chemical potential.

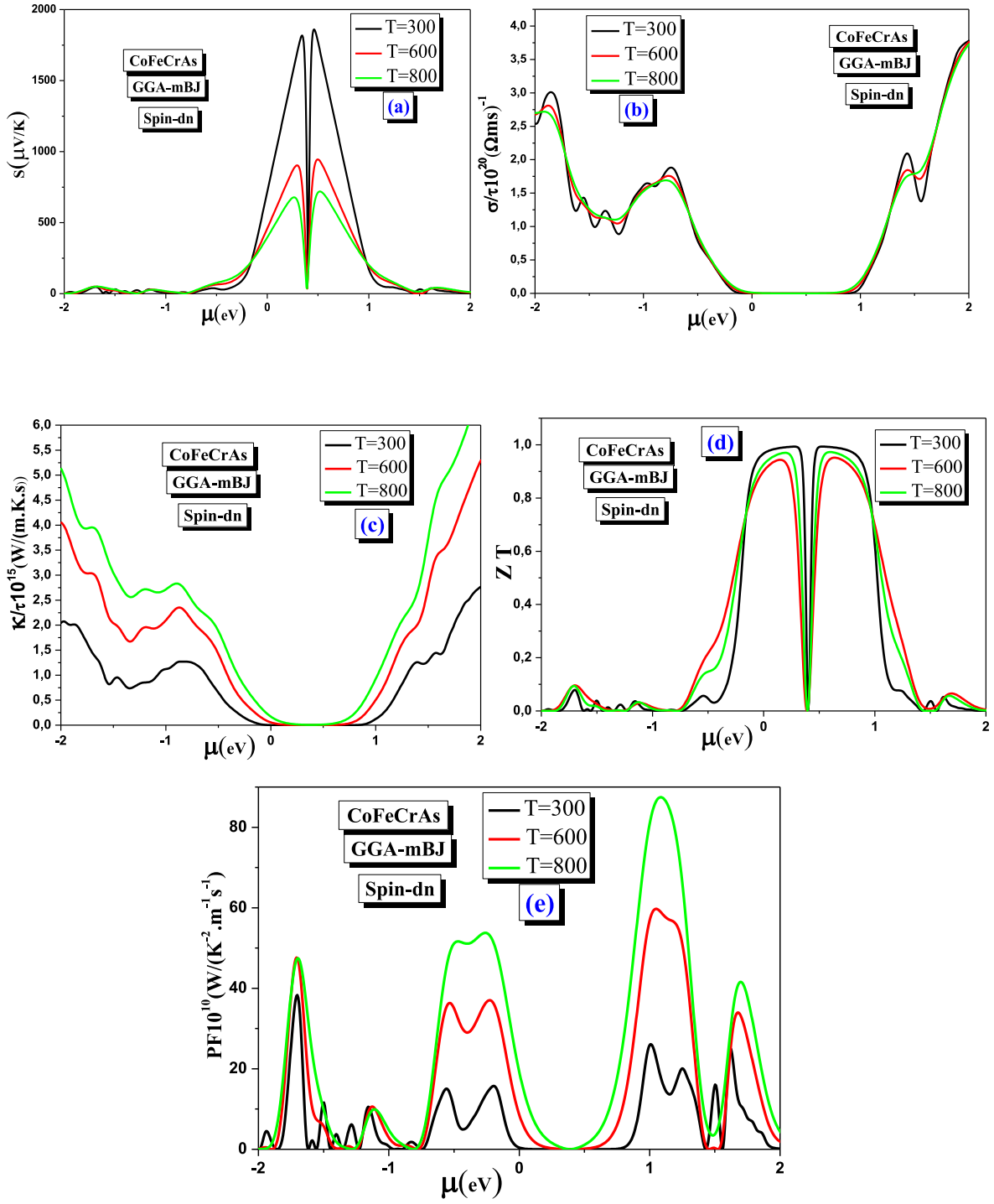


**Fig. 10.** The Seebeck coefficient (a), electrical conductivity (b), electronic thermal conductivity (c), figure of merite (d), Power factor (e) as a function of chemical potential for CoFeCrAs spin dn.

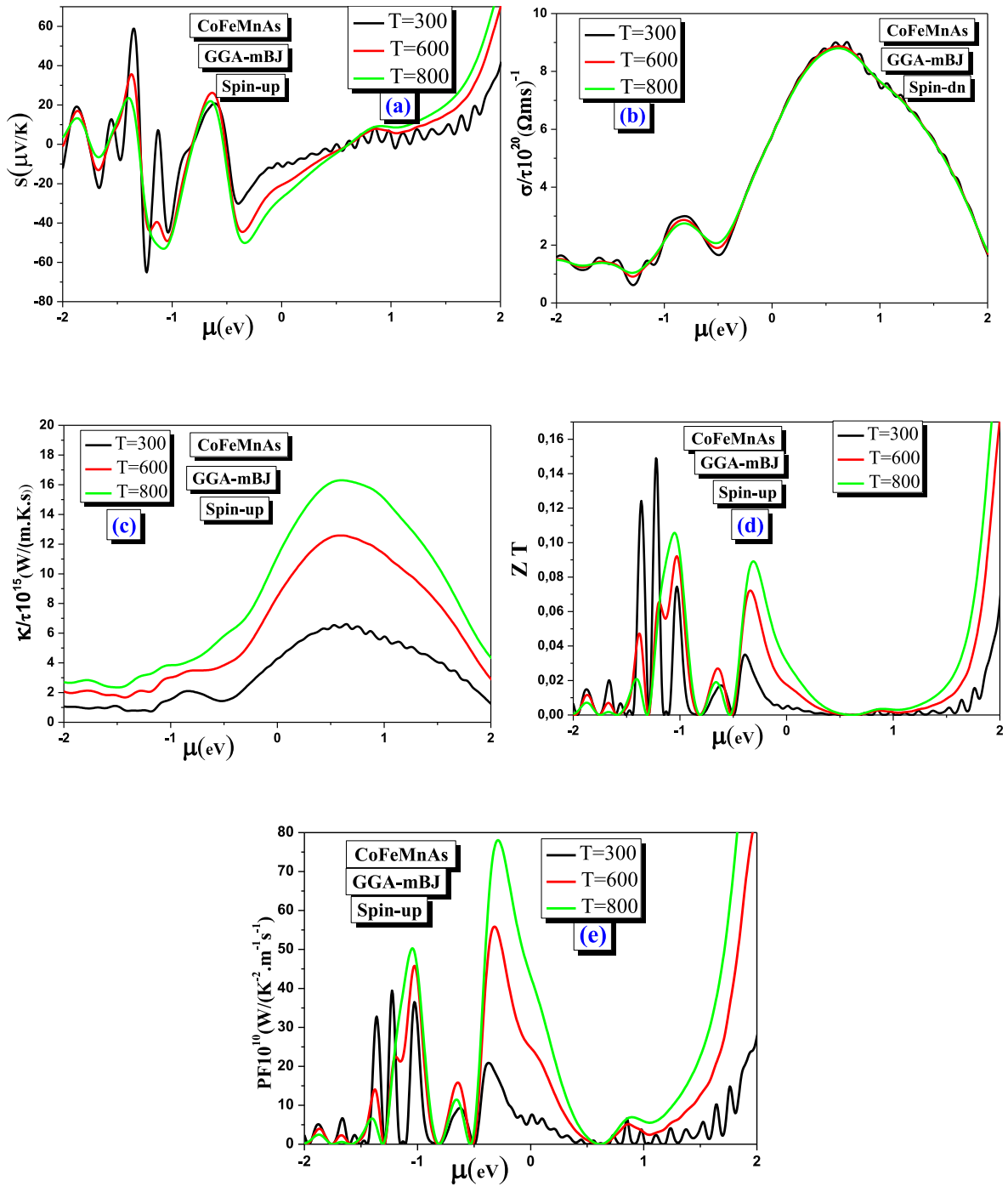


**Fig. 11.** The Seebeck coefficient (a), electrical conductivity (b), electronic thermal conductivity (c), figure of merite (d), Power factor (e) as a function of chemical potential for CoFeMnAs spin up.

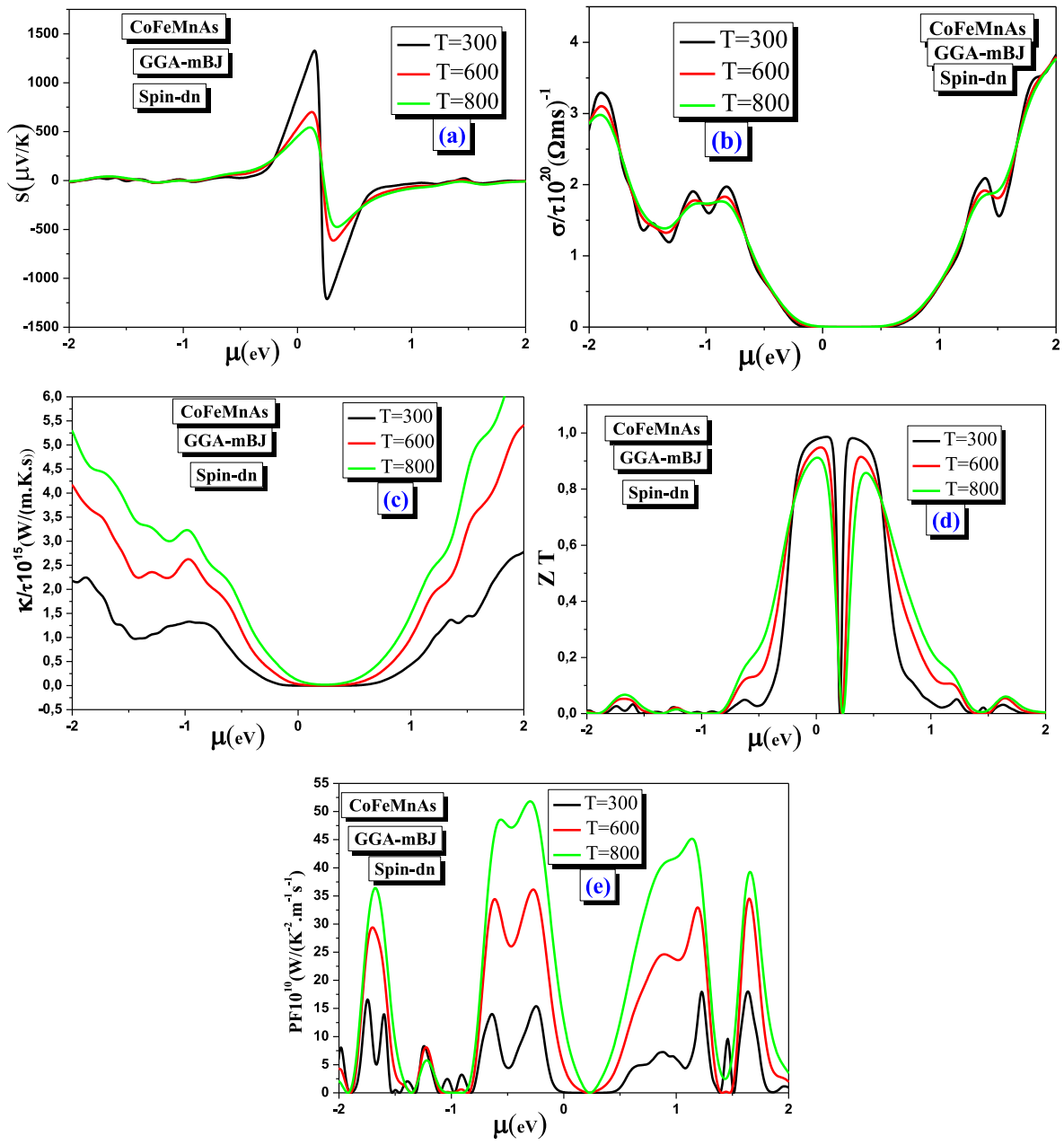


**Fig. 12.** The Seebeck coefficient (a), electrical conductivity (b), electronic thermal conductivity (c), figure of merit (d), and power factor (e) as a function of chemical potential for CoFeMnAs spin dn.

part occupies the part above the Fermi level. There are therefore a total of 3 electrons occupied in the majority-spin channel for Cr. In the minority-spin channel turn, only the d-t2g subshell is occupied. So the Cr offers 2 μB contribution of the magnetic moment as a function of the difference of occupied electrons in the majority-spin and minority-spin channels. Finally, the total magnetic moment for CoFeCrAs is 4 μB.

For the electron spin polarization (SP) at Fermi level ($E_F$) of a material is defined by

$$SP = \frac{N(E_F)^{\uparrow} - N(E_F)^{\downarrow}}{N(E_F)^{\uparrow} + N(E_F)^{\downarrow}} \quad (3)$$

where, $N(E_F)^{\uparrow}$ and $N(E_F)^{\downarrow}$ are the majority-spin and minority-spin densities of states at the Fermi level $E_F$. Total electron density $N(E_F)$ for majority-spin and minority-spin at the Fermi level and spin polarization (SP) for CoFeXAs (X = Cr, Mn and V) alloys calculated using GGA, EV-GGA and mBJ-GGA are reported in Table 8. It can be interpreted from the results of the electron spin polarization at $E_F$ that the 100% spin polarization of CoFeXAs (X = Cr and Mn) alloys is obtained when the Coulomb interaction is considered. Then these two alloys are fully spin polarized and called half-metallic. For CoFeVAs, the spin polarization is located in the range 94–98%.

### 3.5. Thermoelectric properties

We report the effect of chemical potential, temperature and spin on thermoelectric properties of CoFeXAs alloys (X = Cr, Mn and V). The main characteristics of a thermoelectric material are lattice stability, high figure of merit (ZT) and electron spin polarization (SP). The effect of spin, chemical potential and temperature on thermal transport coefficients (Seebeck, electrical conductivity, thermal electronic conductivity, figure of merit and power factor) are reported in Figs. 9–14 using GGA-mBJ functional. Seebeck coefficient called thermoelectric

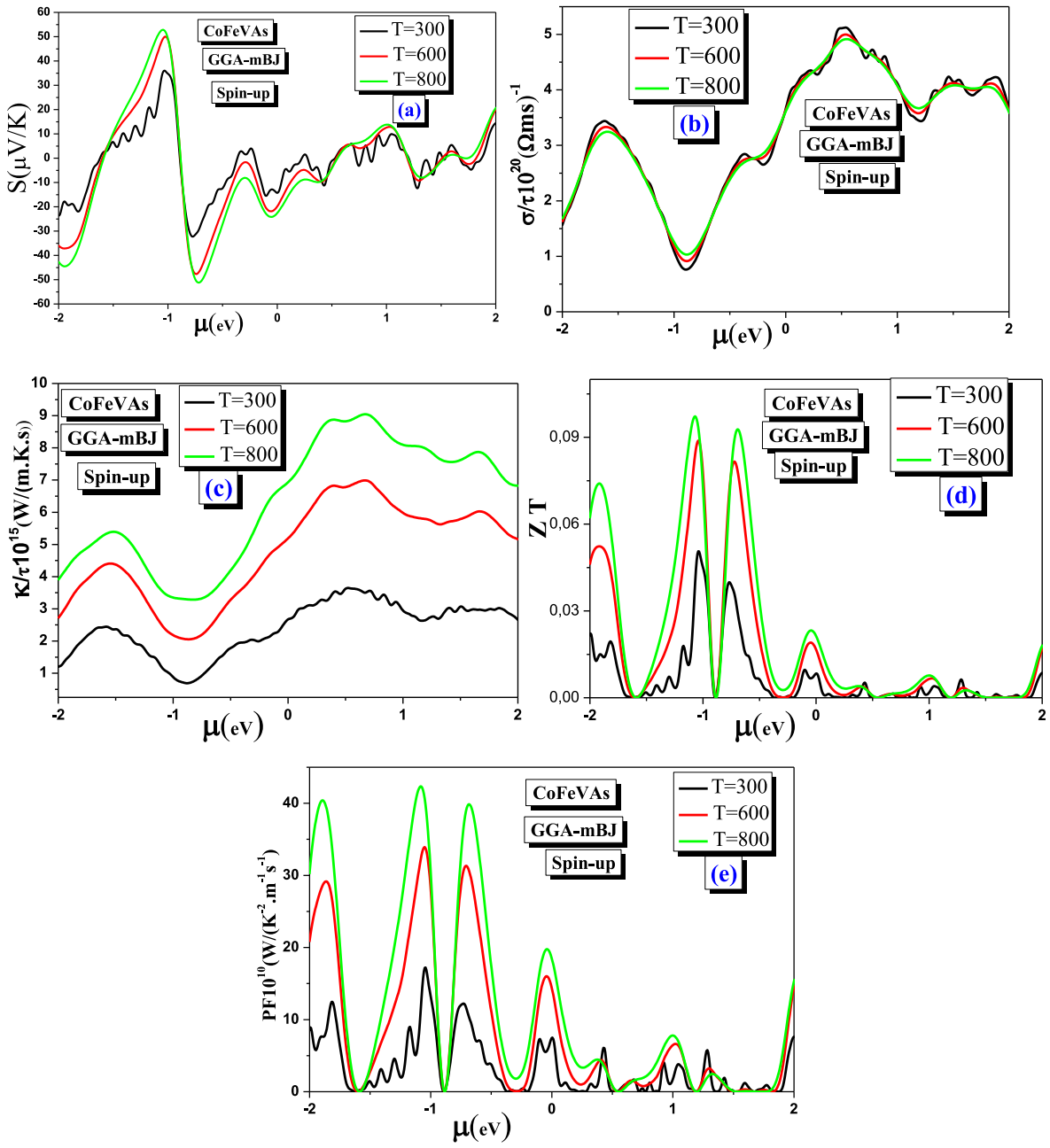


**Fig. 13.** The Seebeck coefficient (a), electrical conductivity (b), electronic thermal conductivity (c), figure of merit (d), and power factor (e) as a function of chemical potential for CoFeVAs spin up.

sensitivity is a measure of the magnitude of the voltage induced across a material under temperature difference effect. Seebeck coefficient of half-metallic material is calculated by the following model:

$$S = \frac{S_{\uparrow}\sigma_{\uparrow} + S_{\downarrow}\sigma_{\downarrow}}{\sigma_{total}} \tag{4}$$

where $\boldsymbol{\sigma}_{total} = (\boldsymbol{\sigma}_{\uparrow} + \boldsymbol{\sigma}_{\downarrow})$ is the total electrical conductivity and $S_{\uparrow}(S_{\downarrow})$ and $\boldsymbol{\sigma}_{\uparrow}(\boldsymbol{\sigma}_{\downarrow})$ are the Seebeck coefficient and electrical conductivity for the majority-spin (minority-spin) channel. For both spin, the increase in temperature reduces the Seebeck coefficient of all studied alloys. The alloys under study present a Seebeck coefficient around the Fermi level having a greater magnitude in the case of the minority-spin. The positive chemical potential corresponds to n-type doping and negative chemical potential for p-type carriers. The fairly high Seebeck in the minority-spin compared to that of majority-spin is related to the flat band structure around the Fermi level in the minority-spin chanel and their half-metallic structure. This behavior is also explained by the large band gap in the case of the minority-spin and thus the electrons are excited to the conduction band. Another explanation is that the dispersion in the valence band is more intense than that in the conduction band near the Fermi level. The negative (positive) value of Seebeck suggests the presence of n-type (p-type) charge carriers [30]. The negative value of Seebeck in a material for minority-spin suggests that the electrons dominate in this chanel. The figure of merit assesses the compatibility of heat transfer and electrical transport. The figure of merit is higher in the case of the minority-spin than in the case of the majority-spin. Each Heusler exhibits two comparable figures of merit peaks for minority-spin, one for n-type and the other for p-type, indicating that these materials have the same thermoelectric efficiency. The contribution of n-type carriers to the majority-spin is insignificant. The n-type's overall electrical conductivity rises quicker than the n-type's. Electrical

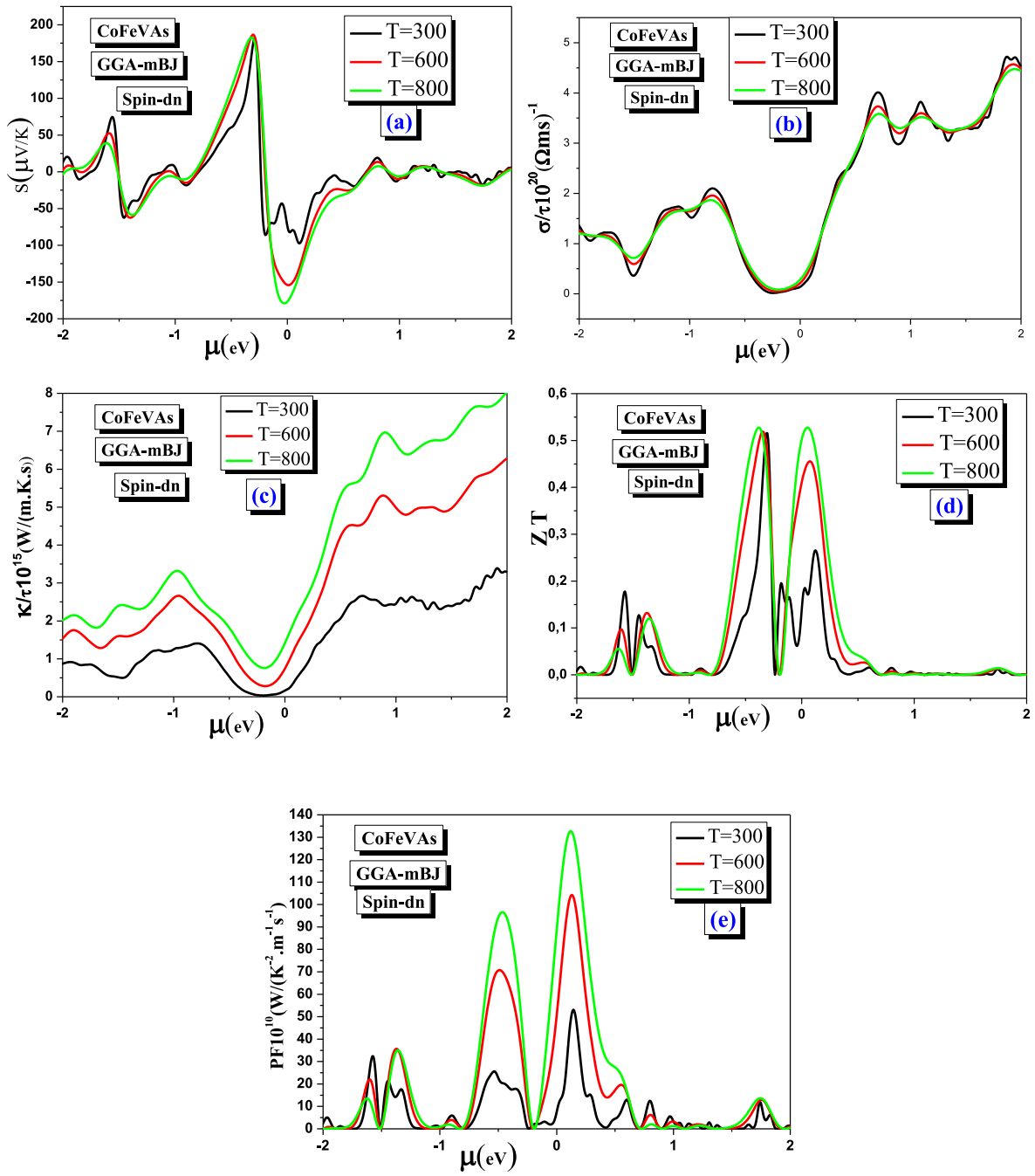


**Fig. 14.** The Seebeck coefficient (a), electrical conductivity (b), electronic thermal conductivity (c), figure of merit (d), and power factor (e) as a function of chemical potential for CoFeVAs spin dn.

conductivity spectra are less temperature sensitive. The maximum electrical conductivity in the minority-spin for the n-type carriers is $\sigma/\tau = 3.7 \times 10^{20}\ (\Omega\ \mathrm{m\ s})^{-1}$, $\sigma/\tau = 3.7 \times 10^{20}\ (\Omega\ \mathrm{m\ s})^{-1}$, and $4.7 \times 10^{20}\ (\Omega\ \mathrm{m\ s})^{-1}$ for CoFeCrAs, CoFeMnAs and CoFeVAs. The increase of temperature enhances the electronic conductivity, where the rate is more significant for the n-type carriers. Fermi level corresponds to undoing material. The $(\sigma/\tau)$ and $(\kappa_e/\tau)$ show a typical semiconductor like behavior. The spectra of the form factor relating to the majority and minority charge carriers are symmetrical for the majority-spin and minority-spin. The highest power factor affirms the general trend of thermoelectric efficiency of materials. The power factor increases with increasing temperature. These alloys have strong spin polarization, a wide direct band gap, a sufficient Seebeck coefficient, and strong UV absorption, making them potential candidates for spintronic and thermoelectric device applications.

## 4. Conclusion

The ab-initio calculation using the FP-LAPW method is used to predict all properties of CoFeVAs, CoFeMnAs and CoFeCrAs using GGA-mBJ exchange-correlation functional. The band gap of CoFeVAs, CoFeMnAs and CoFeCrAs for the minority-spin chanel using GGA-mBJ functional is 0, 0.76 and 1.1 eV. The room temperature absolute Seebeck coefficient with minority-spin for CoFeCrAs, CoFeMnAs and CoFeVAs at 300 K, 600 K and 800 K approaches are 1750, 800 and 600 μV/K, 1250, 750 and 500 μV/K and 175, 175 and 175 μV/K. Our study is a first quantitative theoretical prediction of all studied properties of these alloys. CoFeXAs (X = Cr and Mn) alloys are fully spin-polarized and therefore called half-

metallic. The highest power factor affirms the general trend of thermoelectric efficiency of these studied materials. Alloys under study with half-metallic stability, direct band gap in the minority-spin, high conductivity and absorption in the ultraviolet region, high spin polarization, adequate Seebeck coefficient are candidates for use in solar panels, spintronic and thermoelectric device applications. In these materials, magnetism abides by the Slater-Pauling law. Each atom's partial magnetic moment and the interstitial zone for each alloy contribute to the overall magnetic moment. Vanadium has an antiparallel magnetic moment compared to parallel magnetic moments for Co, Fe, and Mn. The parallel magnetic moments of Co, Fe, Cr, and Mn cause ferromagnetic interactions amongst these atoms, making the alloys under investigation ferromagnetic in nature.

## Authors statements

Conceptualization: Bouferrache, Data curation: M. Ghebouli, Formal analysis:B. Ghebouli, Methodology:T. Chihi, Software:M. Ghebouli and Elkenany B. Elkenany, Validation: Saif A. Mouhammad, Visualization: Norah Algethami, Sultan Alomairy, Roles/Writing - original draft: M. Fatmi, Writing - review & editing: M. Fatmi, Y. Slimani.

## Declaration of competing interest

The author(s) declared no potential conflicts of interest with respect to the research, authorship, and/or publication of this article.

## Data availability

No data was used for the research described in the article.

## Acknowledgement

The researchers would like to acknowledge deanship of scientific research, Taif University for funding this work.

## References

[1] T.M. Bhat, D.C. Gupta, J. Phys. Chem. Solid. 112 (2018) 190–199.
[2] R.A. De Groot, F.M. Mueller, P.G. Van Engen, K.H. JBuschow, Phys. Rev. Lett. 50 (1983) 2024.
[3] T. Graf, C. Felser, S.S.P. Parkin, Prog. Solid State Chem. 39 (2011) 1.
[4] X. Dai, G. Liu, G.H. Fecher, C. Felser, Y. Li, H. Liu, J. Appl. Phys. 105 (2009), 07E901.
[5] G.Y. Gao, Lei Hu, K.L. Yao, Bo Luo, Na Liu, J. Alloys Compd. 551 (2013) 539–543.
[6] H. Rached, D. Rached, R. Khenata, B. Abidri, M. Rabah, N. Benkettou, S.B. Omran, J. Magn. Magn Mater. 379 (2015) 84–89.
[7] F. Dahmane, Y. Mogulkoc, B. Doumi, A. Tadjer, R. Khenata, S. Bin Omran, D.P. Rai, G. Murtaza, D. Varshney, J. Magn. Magn Mater. 407 (2016) 167–174.
[8] X.P. Wei, Y.L. Zhang, T. Wang, X. Sun, T. Song, P. Guo, J. Deng, Mater. Res. Bull. 86 (2017) 139–145.
[9] Y.J. Zhang, Z.H. Liu, Z.G. Wu, X.Q. Ma, Search IUCr J. 6 (2019) 610–618.
[10] K. Inomata, N. Ikeda, N. Tezuka, R. Goto, S. Sugimoto, M. Wojcik, E. Jedryka, Sci. Technol. Adv. Mater. 9 (2008), 014101.
[11] C. Felser, G.H. Fecher, B. Balke, Angew. Cem., Int. Ed. 46 (2007) 668.
[12] K. Özdoğan, E. Şaşıoğlu, I. Galanakis Citation, J. Appl. Phys. 113 (2013), 193903.
[13] R. Jain, V. Jain, A.R. Chandra, V. Jain, N. Lakshmi, J. Supercond. Nov. Magnetism 31 (2018) 2399–2409.
[14] A. Bahnes, A. Boukortt, H. Abbassa, D.E. Aimouch, R. Hayn, A. Zaoui, J. Alloys Compd. 731 (2018) 1208–1213.
[15] P. Blaha, K. Schwarz, G.K.H. Madsen, D. Kvasnicka, J. Luitz, R. Laskowsk, F. Tran, L. Marks, L. Marks, Mater. Sci. Eng. (2019).
[16] J.P. Perdew, K. Burke, M. Ernzerhof, Phys. Rev. Lett. 77 (1996) 3865.
[17] A.D. Becke, E.R. Johnson, A Simple Effective Potential for Exchange, American Institute of Physics, 2006.
[18] V.I. Anisimov, O. Gunnarsson, Phys. Rev. B 43 (1991) 7570.
[19] Georg K.H. Madsen, Pavel Novák, Europhys. Lett. 69 (2005) 777.
[20] V.I. Anisirnov, O. Gunnarsson, Phys. Rev. B 43 (10) (1991) 7570.
[21] Botan J. Abdullah, Musafa S. Omar, Nawzat S. Saadi, Qing Jiang, Int. J. Sci. Eng. Res. 6 (2015) 842–846.
[22] T.M. Bhat, D.C. Gupta, J. Magn. Magn Mater. 449 (2018) 493–499.
[23] M.H. Elahmar, H. Rached, D. Rached, R. Khenata, G. Murtaza, S. Bin Omran, W. K. Ahmed, J. Magn. Magn Mater. 393 (2015) 7165–7174.
[24] B. Ghebouli, M.A. Ghebouli, T. Chihi, M. Fatmi, S. Boucetta, M. Reffas, Solid State Commun. 149 (2009) 2244.
[25] O.A. Yassin, Optik 127 (2016) 1817.
[26] M.R. Boufatah, A.E. Merad, Mater. Sci. Semicond. Process. 19 (2014) 179.
[27] K. Bouferrache, M.A. Ghebouli, B. Ghebouli, M. Fatmi, S. Alomairy, T. Chihi, Chin. J. Phys. 81 (2022) 303–324.
[28] L. Krache, M.A. Ghebouli, B. Ghebouli, M. Fatmi, T. Chihi, S.I. Ahmed, Acta Phys. Pol., A 143 (2023) 3–11.
[29] I. Galanakis, P.H. Dederichs, N. Papanikolaou, Phys. Rev. B 66 (2002), 174429.
[30] L. Jingyu, Z. Guangbiao, P. Chengxiao, W. Wenxuan, Y. Jinfeng, W. Yuanxu, C. Zhenxiang, Phys. Chem. Chem. Phys. 10 (2019) 5803–5812.